

QCD Loop Corrections to Top Production and Decay at e^+e^- Colliders

Cosmin Macesanu ¹

*Department of Physics and Astronomy, University of Rochester
Rochester, NY 14627-0171, USA*

*Department of Physics, Oklahoma State University ²
Stillwater, OK 74078, USA*

Abstract

We present a computation of QCD next-to-leading order virtual corrections to the top production and decay process at linear colliders. The top quarks are allowed to be off-shell and the production and decay subprocesses are treated together, thus allowing for interference effects. The framework employed for our computation is the double pole approximation (DPA). We describe the implementation of this approximation for the top production and decay process and compare it with the implementation of DPA for the evaluation of QED corrections to the W pair production at LEP II. Similarities and differences between the two cases are pointed out. One result of interest is the incomplete cancelation of interference corrections. Other results include values for the total NLO top production cross section, and the impact the nonfactorizable (interference) corrections have on the top invariant mass distribution.

1 Introduction

The top quark might prove to be one of the most interesting elementary particles discovered so far. Since its mass is so large (close to the electroweak symmetry breaking scale), it can be assumed that study of top properties will allow us to learn new things about the physics at the next energy scale. So far, though, due to low statistics in the Run I at Tevatron, our knowledge of the top quark is rather limited. Future runs at the Tevatron and the LHC will provide more information, but the analysis of this new data will be complicated by large QCD backgrounds.

An e^+e^- collider with center-of-mass energy at and above the top threshold promises to provide a clean environment in which to perform precision studies of the top quark [1]. Indeed, it is conceivable that at such a machine the study of top can be performed with a

¹Email address: mcos@pas.rochester.edu

²Current address.

precision similar to that achieved in the study of the W boson at LEP II. This means order % (and better) measurements of differential cross sections for processes involving the top quark. Such a precision in measuring experimental quantities implies the need for a like precision in our theoretical understanding of these processes. This in turn requires the inclusion of radiative corrections in our predictions.

A wealth of information about the top quark (like its mass, width, strong and Yukawa coupling constants) can be extracted from measurements performed at the production threshold. For this region, comprehensive theoretical studies (NNLO computation with resummation of large logarithms, careful treatment of the renormalon ambiguity) have already been performed ([2] and references therein). Going to higher energies, we can study the V-A structure of the top quark couplings to the gauge bosons (γ , Z and W) [3]. The information about couplings can be obtained by using spin correlations: the top quarks are produced in certain spin states, as dictated by the top - γ , Z couplings. Since the top decays before hadronization, the spin states of the top directly influence the angular distributions of its decay products. Simulations show that by analyzing kinematic variables of final state particles it is possible to measure the top-gauge boson couplings at the several percent level [1].

The subject of this paper is the evaluation of NLO QCD corrections to the top production and decay process above threshold at a Linear Collider. Previous work in this area includes the study of corrections to the top production subprocess, with virtual and soft gluons [4] as well as with hard gluon radiation ([5], [6], [7] are just some examples), and to the top decay subprocess with virtual and hard gluons together ([8], [9], [10]).

Using these results, one can try to understand the top production and decay process by assuming that the intermediate top quarks are on-shell (narrow width approximation) and treating the subprocesses separately [11]. This assumption is usually reasonable; the result for the total cross section is valid up to terms of order $\Gamma_t/m_t \sim 1\%$. However, the effects of finite top width can be important in some differential cross sections; and if precision better than percent level is needed, the production and decay processes have to be considered together, by allowing the top quark to go off-shell. These corrections can be thought of as being due to interference between production and decay, and are also known as nonfactorizable corrections. Some results concerning the nonfactorizable corrections for the top production process have already been published [12]; we present here a more complete analysis.

We shall perform this computation and present the results at the parton level only. We assume that the issues related to jet reconstruction and identification can be solved, and the final state contains two W bosons ³ and two b quarks (the real gluon radiation case has been analyzed in [13], [14]). Even at this level, the complete computation of all the diagrams contributing to this final state (Born and next to leading order) is a very difficult task. Therefore, we shall employ the double pole approximation (DPA) which means taking into account only the diagrams which contain a top - antitop pair.

Here, it is worth mentioning the strong similarities between the evaluation of QCD cor-

³ At the Monte Carlo level, we actually allow the on-shell W 's to decay, either semileptonically or into a pair of massless quarks, but in the latter case we do not take into consideration QCD corrections to the W decay.

rections to the process of interest to us:

$$e^+e^- \rightarrow t \bar{t} \rightarrow b W^+ \bar{b} W^- \quad (1)$$

and the evaluation of QED corrections to the W pair production and decay process ($e^+e^- \rightarrow W^+ W^- \rightarrow 4f$) at LEP. The issues which arise in the two computations are similar, because in both cases we are dealing with the production and decay of heavy unstable particles. Our treatment is largely similar to the one used for the electroweak process [15], [16], [18]. But there are some differences, both in the implementation of the DPA approximation and in the number and type of terms which contribute to the final result (the latter being due to the fact that in our case the intermediate off-shell particles are fermions, and not bosons). These differences will be pointed out in the course of our discussion.

The outline of the paper is as follows. In sect. 2 we lay out in some detail the theoretical framework in which we perform our computation. This includes a short description of the DPA method, with examples of evaluation of NLO amplitudes in this approximation. The main point of this section is that the results for the amplitudes corresponding to interference diagrams are similar to results previously obtained for the W pair production process, while for the vertex corrections and fermion self-energy diagrams there are differences between the two cases. In order to facilitate comparisons with the on-shell approach, we also formulate our results in terms of corrections to the production and decay subprocesses and interference contributions. The gauge invariance of the total and partial amplitudes in DPA is manifest in this formulation. Sect. 3 contains some details on the design of the Fortran code we used to obtain our numerical results, which are presented in sect. 5. A short discussion of a slightly different approach in evaluating the non-factorizable corrections (used in [12]) is presented in sect. 4. We end with the conclusions.

2 Amplitudes in DPA

Since it decays very fast, the top quark is not studied directly, but through its decay products. In top pair production at linear colliders, the relevant process is:

$$e^+e^- \rightarrow b W^+ \bar{b} W^- \quad (2)$$

At tree level, the diagrams contributing to this process can be split into 3 classes: diagrams which contain a top-antitop pair (Fig. 1), diagrams which contain either one top quark or a top antiquark (Fig. 2 and charge conjugates), and diagrams which do not contain any top (there are about 50 such diagrams). The evaluation of all these amplitudes can be performed using one of the automated tree level amplitude computation programs, like MADGRAPH ([19], see also [20]). The computation of QCD corrections to all tree level diagrams, however, increases the degree of complexity by quite a lot, and is probably not feasible yet.

Hence the need to use some methods which will simplify the computation, but will provide approximate results for the virtual corrections. One such method is the *double pole approximation* (DPA), which makes use of the fact that, looking for top pair production, we are interested in a specific region of the final state phase space of (2). This region is defined by the requirement that the invariant mass of the $W b$ pair is close to the top mass:

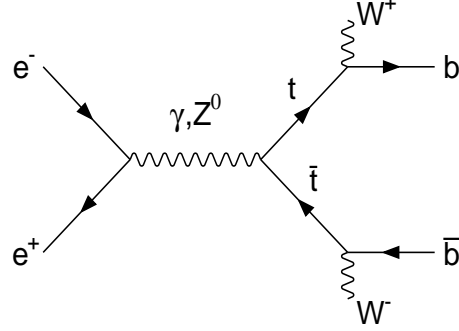


Figure 1: The top-antitop diagrams contributing to the process (2).

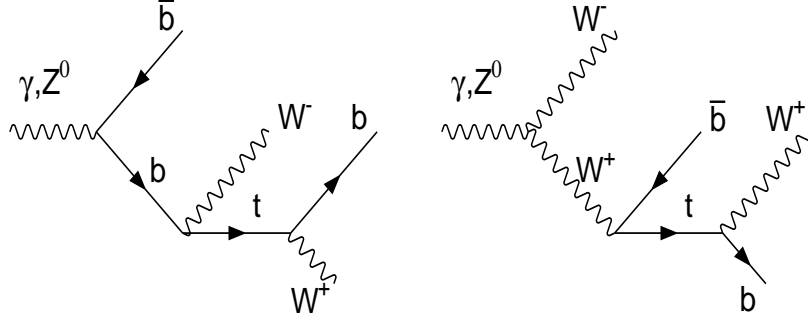


Figure 2: Single top diagrams contributing to the process (2).

p_t^2 , $p_{\bar{t}}^2 \approx m_t^2$, where $p_t = p_{W^+} + p_b$ and $p_{\bar{t}} = p_{W^-} + p_{\bar{b}}$. In this region, the amplitudes corresponding to the top-antitop diagrams are enhanced by the two resonant propagators coming from the two intermediate top quarks⁴:

$$\mathcal{M} \sim \frac{1}{p_t^2 - \bar{m}_t^2} \frac{1}{p_{\bar{t}}^2 - \bar{m}_t^2} \quad (3)$$

(the diagrams in (Fig. 1) are therefore called doubly resonant) and we can neglect the contributions coming from the singly resonant diagrams (Fig. 2) or nonresonant ones, which are *reduced* by factors of (Γ_t/m_t) or $(\Gamma_t/m_t)^2$ with respect to the doubly resonant contributions.

The real gluon corrections to the doubly resonant diagrams have been computed in [13]. The aim of this paper is the DPA evaluation of the virtual corrections to the top production and decay process. Some of Feynman diagrams contributing to these corrections are presented in Figure 3. These diagrams can be roughly divided into two classes : corrections to particular subprocesses – the vertex and fermion self-energy diagrams in Fig. 3 a) and b) respectively – and interference type corrections (Fig. 3 c) and d)). Strictly speaking, the vertex and self-energy diagrams also contribute to interference between subprocesses; but,

⁴We use the notation $\bar{m}_t^2 = m_t^2 - im_t\Gamma_t$

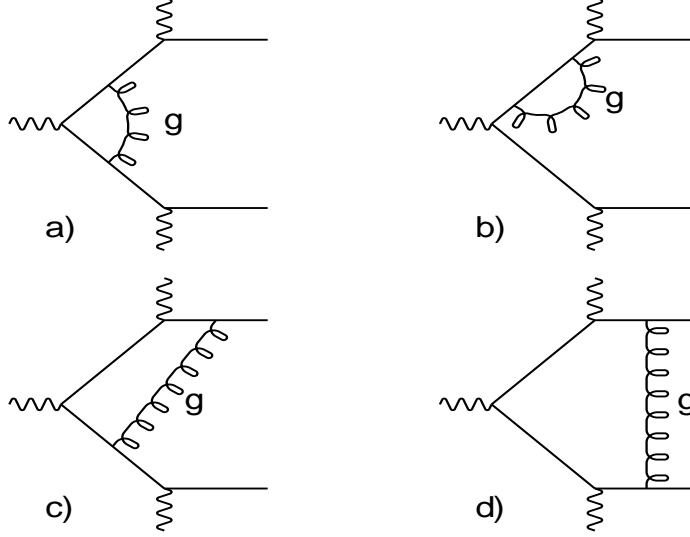


Figure 3: Feynman diagrams for virtual gluon corrections to top production and decay.

for the sake of brevity, we shall refer to the diagram in Fig. 3 a) as the production vertex correction diagram, and so on. Also, in the following, we will denote the tree level amplitude (Fig. 1) by \mathcal{M}^0 , and the amplitude for the first order virtual corrections by \mathcal{M}^{vg} :

$$\mathcal{M}^{vg} = \mathcal{M}_{t\bar{t}} + \mathcal{M}_{tb} + \mathcal{M}_{t\bar{b}} + \mathcal{M}_{b\bar{t}} + \mathcal{M}_{t\bar{b}} + \mathcal{M}_{b\bar{b}} \quad (4)$$

Here, the first three terms correspond to the three off-shell vertex corrections (which include in a suitable way the fermion self-energies, as described in section 2.4), and the last three terms come from the interference diagrams.

2.1 Interference diagrams

We start by discussing the evaluation of interference diagrams in Figs. 3c), 3d). Technically, this is one of the more involved computations we have to perform. The full evaluation of the $\bar{t} - b$ interference amplitude⁵:

$$\begin{aligned} \mathcal{M}_{b\bar{t}} = \bar{u}(b) & \left[(-ig_s^2) \int \frac{d^4 k}{2\pi^4} \frac{1}{k^2 + i\epsilon} \gamma^\mu \frac{\not{p}_b - \not{k} + m_b}{(p_b - k)^2 - m_b^2} \not{\epsilon}_{W^+} \frac{\not{p}_t - \not{k} + m_t}{(p_t - k)^2 - m_t^2} \Gamma_{\gamma, Z_0} \right. \\ & \left. \times \frac{-\not{p}_{\bar{t}} - \not{k} + m_{\bar{t}}}{(p_{\bar{t}} + k)^2 - m_{\bar{t}}^2} \gamma_\mu \right] \frac{-\not{p}_{\bar{t}} + m_{\bar{t}}}{p_{\bar{t}}^2 - m_{\bar{t}}^2} \not{\epsilon}_{W^-} v(\bar{b}) \end{aligned} \quad (5)$$

is, for example, quite a difficult task. However, the only terms of interest to us in DPA are those which have resonances at the top and antitop quark propagator poles. This simplifies our task greatly. The doubly resonant terms can be extracted with the help of the following observation: if the virtual gluon in the loop is hard, then the quantity in brackets does

⁵The Feynman gauge is used for the gluon propagator.

not have any singularity, and the overall resonant structure for this diagram is given only by the pole due to the antitop propagator: $\mathcal{M}_{b\bar{t}}(\text{hard gluon}) \propto 1/(p_t^2 - \bar{m}_t^2)$. This means that any doubly resonant terms contribution to $\mathcal{M}_{b\bar{t}}$ are entirely due to soft virtual gluons. Therefore, we can neglect the k terms in the numerator of (5). Following [16], we shall call this approximation the *extended soft gluon approximation* (ESGA) ⁶.

With the help of the transformations:

$$\gamma^\mu (\not{p}_b + m_b) = (-\not{p}_b + m_b) \gamma^\mu + 2p_b^\mu \rightarrow 2p_b^\mu \quad (6)$$

$$(-\not{p}_{\bar{t}} + m_t) \gamma_\mu = \gamma_\mu (\not{p}_{\bar{t}} + m_t) - 2p_{\bar{t}\mu} \rightarrow -2p_{\bar{t}\mu}$$

(the term $(\not{p}_{\bar{t}} + m_t)$ on the second line is neglected, since it would lead to a singly resonant contribution), the following result is obtained for the amplitude (5):

$$\begin{aligned} \mathcal{M}_{b\bar{t}}(DPA + ESGA) &= \frac{\alpha_s}{4\pi} \mathcal{M}_0 \times (-4p_b p_{\bar{t}})(p_t^2 - \bar{m}_t^2) \\ &\times \int \frac{d^4 k}{i\pi^2} \frac{1}{k^2 + i\epsilon} \frac{1}{k^2 - 2kp_b} \frac{1}{(p_t - k)^2 - \bar{m}_t^2} \frac{1}{(p_{\bar{t}} + k)^2 - \bar{m}_t^2} \end{aligned} \quad (7)$$

The result is proportional to the tree level amplitude – in the DPA, the virtual corrections due to interference factorize. The proportionality factor includes the scalar 4-point function (the integral on the second line of Eq. (7)) $\mathcal{D}_{b\bar{t}}^0 = \mathcal{D}^0(-p_b, -p_t, p_{\bar{t}}, 0, m_b, \bar{m}_t, \bar{m}_t)$. ⁷

Let's discuss shortly the resonant behavior of the DPA amplitude in (7). Apparently, the result for $\mathcal{M}_{b\bar{t}}$ has a single pole at $p_t^2 = m_t^2$ (the other pole being canceled by the multiplicative term $p_t^2 - m_t^2$). However, if the top (or antitop) goes on-shell, the \mathcal{D}^0 function acquires an infrared singularity (in the zero top width limit; this singularity is regularized by the top width). Since the infrared singular type terms have a logarithmic structure (this can also be reasoned from power counting arguments), this indicates that \mathcal{D}^0 has the following behavior close to the top resonances:

$$\mathcal{D}_{b\bar{t}}^0 \sim a_1 \log(p_t^2 - \bar{m}_t^2) + a_2 \log(p_{\bar{t}}^2 - \bar{m}_t^2) \quad (8)$$

Here a_1 and a_2 are terms which are finite when *either* the top or antitop quark go on-shell. Formally, then, the overall resonant behavior of the interference amplitude $\mathcal{M}_{b\bar{t}}$ in DPA is

⁶In the standard soft gluon approximation, k^2 terms in the denominator of top quark propagators would also be neglected; we do not do this here for computational reasons (see also [16], [21]).

⁷ For the scalar one-loop integrals appearing here we use the following notation:

$$\begin{aligned} \mathcal{D}^0(p_1, p_2, p_3, m_0, m_1, m_2, m_3) &= \int \frac{d^4 k}{i\pi^2} \frac{1}{N_0 N_1 N_2 N_3} \\ \mathcal{E}^0(p_1, p_2, p_3, p_4, m_0, m_1, m_2, m_3, m_4) &= \int \frac{d^4 k}{i\pi^2} \frac{1}{N_0 N_1 N_2 N_3 N_4} \end{aligned}$$

with the denominators :

$$N_0 = k^2 - m_0^2 + i\epsilon, \quad N_i = (k + p_i)^2 - m_i^2 + i\epsilon, \quad i = 1, \dots, 4$$

of type $pole \times logarithm$:

$$\mathcal{M}_{b\bar{t}} \sim \tilde{\mathcal{M}}_0 \log(p_t^2 - \bar{m}_t^2) \frac{1}{p_t^2 - \bar{m}_t^2}$$

rather than $pole \times pole$, as it is for the tree level amplitude or for the corrections to production or decay subprocesses.

Using the same techniques, similar results are easily obtained for the other two interference diagrams. In the soft gluon approximation (and DPA):

$$\mathcal{M}_{t\bar{b}}(DPA + ESGA) = \frac{\alpha_s C_F}{4\pi} \mathcal{M}_0 \times (-4p_t p_{\bar{b}})(p_t^2 - \bar{m}_t^2) \mathcal{D}_{t\bar{b}}^0 \quad (9)$$

$$\mathcal{M}_{b\bar{b}}(DPA + ESGA) = \frac{\alpha_s C_F}{4\pi} \mathcal{M}_0 \times (-4p_b p_{\bar{b}})(p_t^2 - \bar{m}_t^2)(p_t^2 - \bar{m}_t^2) \mathcal{E}_{b\bar{b}}^0 \quad (10)$$

where $\mathcal{D}_{t\bar{b}}^0 = \mathcal{D}^0(-p_{\bar{b}}, -p_{\bar{t}}, p_t, 0, m_b, \bar{m}_t, \bar{m}_t)$ and

$$\mathcal{E}_{b\bar{b}}^0 = \mathcal{E}^0(-p_b, -p_t, p_{\bar{t}}, p_{\bar{b}}, \mu, m_b, \bar{m}_t, \bar{m}_t, m_b) \quad (11)$$

is the scalar 5-point function (here μ is the infinitesimally small gluon mass needed for the regularization of infrared divergent behavior of $\mathcal{E}_{b\bar{b}}^0$).

We end this section with some comments on the numerical magnitude of interference terms. Since the resonant behavior of these terms is of $pole \times log$ type, it might be expected that they are less important numerically than the double pole terms. However, analytic expressions for the \mathcal{D}_0 function ([16], [17], [18]) show that, although the coefficients a_1, a_2 in (8) are finite when one of the top or antitop quark goes on shell, they will diverge when both particles go on-shell simultaneously:

$$a_i \sim \frac{1}{c_{1i}(p_t^2 - \bar{m}_t^2) + c_{2i}(p_{\bar{t}}^2 - \bar{m}_t^2)}$$

Therefore, the leading logarithms in the scalar 4 and 5-point functions will be enhanced by factors of order m_t/Γ_t near the top, antitop quark mass resonances.

2.2 Vertex corrections

The results for the interference diagrams are completely analogous to results obtained in the W pair production computation. However, for the off-shell vertex and self-energy corrections diagrams, the results in the top case are different. Consider for example, the amplitude for the general vertex correction in Figure 4:

$$\delta\Gamma^\mu = \frac{\alpha_s}{4\pi} \int \frac{d^4 k}{i\pi^2} \frac{1}{k^2} \gamma^\nu \frac{\not{p}_1 - \not{k} + m_1}{(p_1 - k)^2 - \bar{m}_1^2} \gamma^\mu (C_V + C_A \gamma^5) \frac{-\not{p}_2 - \not{k} + m_2}{(p_2 + k)^2 - \bar{m}_2^2} \gamma_\nu$$

Upon evaluation (and keeping only the vector part) the result can be written in terms of eight form factors, each of them multiplying a different tensor quantity:

$$\delta\Gamma_V^\mu = \frac{\alpha_s}{4\pi} C_V [\gamma^\mu F_2 + (\not{p}_1 - m_1) \gamma^\mu F_4 + \gamma^\mu (-\not{p}_2 - m_2) F_6]$$

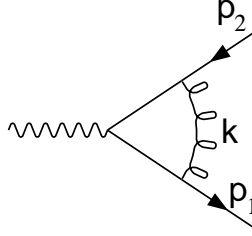


Figure 4: General vertex correction diagram.

$$+(\not{p}_1 - m_1)\gamma^\mu(-\not{p}_2 - m_2)F_8 + p_1^\mu F_1 + (\not{p}_1 - m_1)p_1^\mu F_3 + \dots] \quad (12)$$

(expressions for the scalar form factors F_1, \dots, F_8 can be found in the Appendix). In the on-shell case, only the F_2 (electric dipole) and F_1 (magnetic dipole momentum) form factors contribute. It might be expected that in the double pole approximation we can drop the other terms, too, since they have a zero at $\not{p}_1 = m_1$ (or $\not{p}_2 = -m_2$) which will cancel one pole (or both) in the amplitude. However, the form factors themselves may have a resonant structure when the particles go on shell.

Consider the top decay vertex correction. In this case, $p_1 \rightarrow p_b, p_2 \rightarrow -p_t$, and only four terms survive in Eq. (12); the corresponding form factors contain terms which are proportional to the scalar 3-point function:

$$F_i \sim C_{tb}^0 = \int \frac{d^4 k}{i\pi^2} \frac{1}{k^2} \frac{1}{(p_b - k)^2 - m_b^2} \frac{1}{(p_t - k)^2 - \bar{m}_t^2} \quad i = 1, 2, 5, 6$$

which has a logarithmic resonant behavior:

$$C_{tb}^0 \sim \log(p_t^2 - \bar{m}_t^2).$$

Therefore, the contribution of $i = 5, 6$ terms to the top decay vertex correction is doubly resonant, although of type *pole* \times *log* rather than double pole. Because these logarithms are not multiplied by large factors (as in the case of the interference diagrams), these terms can be expected to be numerically small; for consistency reasons it is still desirable to include them in the final result.

Similar results are obtained for the correction to the antitop decay vertex (we keep the $i = 1, 2, 3, 4$ terms in this case). In the case of the $t - \bar{t}$ vertex, though, both fermions are off-shell; as a consequence, there are no resonant logarithms when either the top or antitop quark goes on-shell, and we keep only the $i = 1, 2$ terms.

It follows that in the general expression (12) it is necessary to keep the terms which contain F_1 to F_6 (the F_7 and F_8 terms can be dropped), and we don't have factorization for the interference part anymore. This is different from what happens in the W pair production process, where the DPA factorization holds even for the vertex corrections. This difference between the two cases is due to the fact that in one process the intermediate particles are fermions, while in the other they are bosons.

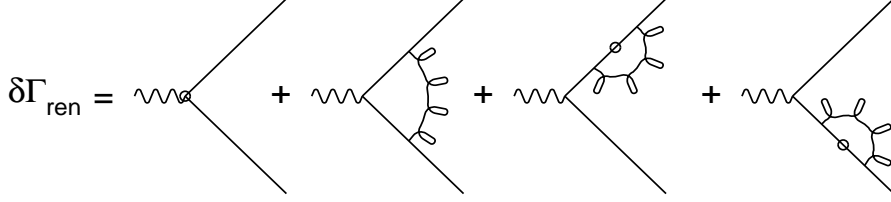


Figure 5: Terms contributing to the renormalized vertex; the dots represent counterterm insertions.

2.3 Renormalization and fermion self-energy

For the renormalization of the ultraviolet divergences appearing in the evaluation of the vertex and fermion self-energy corrections we use the counterterm method. What this amounts to is replacing the bare vertex correction in Fig. 4 (which is UV divergent) with a finite renormalized vertex correction (Fig. 5):

$$\delta\Gamma_{ren}^\mu = \delta\Gamma^\mu + \Gamma^\mu \delta Z_2 + \frac{1}{2}(-i\hat{\Sigma}_2(\not{p}_1)) \frac{i}{\not{p}_1 - m_1} \Gamma^\mu + \frac{1}{2} \Gamma^\mu \frac{i}{-\not{p}_2 - m_2} (-i\hat{\Sigma}_2)(\not{p}_2) \quad (13)$$

which also includes the contributions of the fermion self-energy diagram.

The first two terms in Eq. (13) are what is usually defined as the renormalized vertex. The last two terms are one half of the renormalized fermion and antifermion self-energy:

$$\hat{\Sigma}_2(\not{p}) = \Sigma_2(\not{p}) - (\pm \not{p} - m) \delta Z_2 - \Delta m \quad (14)$$

where δZ_2 and Δm are coefficients of the counterterms in the Lagrangian density (the \pm sign corresponds to the particle/antiparticle case). In the above equation, Σ_2 stands for the *bare* fermion self-energy:

$$\Sigma_2(\not{p}) = \frac{\alpha_s}{4\pi} \int \frac{d^4 k}{i\pi^2} \frac{1}{k^2} \gamma^\mu \frac{\not{p} - \not{k} + m}{(p - k)^2 - \bar{m}^2} \gamma_\mu \quad (15)$$

Upon evaluation, the result for Eq. (15) can be separated into a scalar and a spinorial component:

$$\Sigma(\not{p}) = (\pm \not{p} - m) \Sigma_a(p^2) + m \Sigma_b(p^2)$$

With these notations, the renormalized vertex correction can be written as:

$$\delta\Gamma_{ren}^\mu = \delta\Gamma^\mu + \frac{1}{2} \Delta Z_2(p_1) \Gamma^\mu + \frac{1}{2} \Gamma^\mu \Delta Z_2(p_2) \quad (16)$$

with

$$\Delta Z_2(p) = \Sigma_a(p^2) + \frac{m \Sigma_b(p^2) - \Delta m}{\pm \not{p} - m} \quad (17)$$

The counterterm coefficient Δm is fixed by the on-shell renormalization condition:

$$\hat{\Sigma}_2(\not{p} = m) = 0 \Rightarrow \Delta m = m \Sigma_b(m^2) \quad (18)$$

Also, in the on-shell limit,

$$\Delta Z_2(p)|_{\not{p} \rightarrow m} = \left(\Sigma_a(p^2) + \frac{\partial \Sigma_b(\not{p})}{\partial \not{p}} \Big|_{\not{p} \rightarrow m} \right) = \frac{\partial \Sigma_2(\not{p})}{\partial \not{p}} \Big|_{\not{p} \rightarrow m} = \delta Z_2 \quad (19)$$

where for the last equality we have used the renormalization condition

$$\frac{\partial \hat{\Sigma}_2(\not{p})}{\partial \not{p}} \Big|_{\not{p} \rightarrow m} = 0$$

It is convenient to write the contribution of the fermion self-energy diagrams in a form similar to that of Eq. (12). Using the resummed top quark propagator:

$$\frac{i}{\pm \not{p} - m} \longrightarrow \frac{i(\pm \not{p} + m)}{p^2 - \bar{m}^2} \quad (20)$$

we obtain the following result for ΔZ_2 :

$$\Delta Z_2(p) = \left([\Sigma_a(p^2) + 2\Sigma_{ir}(p^2)] + \frac{\Sigma_{ir}(p^2)}{m}(\pm \not{p} - m) \right) \quad (21)$$

with

$$\Sigma_{ir}(p^2) = m \frac{\Sigma_b(p^2) - \Sigma_b(m^2)}{p^2 - \bar{m}^2}.$$

The term in square brackets in Eq. (21) will multiply the Born cross section. The term proportional to $(\pm \not{p} - m)$ is identical to the like terms appearing in the expression for the vertex correction Eq. (12). Since Σ_{ir} is the part of the self-energy correction which would be infrared divergent on-shell (which means that it has a logarithmic resonant behavior

$$\Sigma_{ir}(p^2) \sim \log(p^2 - \bar{m}^2)$$

in the off-shell case), this term is also kept.

2.4 Gauge invariance and corrections to particular subprocesses

The partial amplitudes appearing in Eq. (4) can be directly related to Feynman diagrams and are straightforward to evaluate. However, as mentioned before, they cannot be directly identified with corrections to particular subprocesses. For example, the top - antitop production vertex diagram (Figure 3a)) contributes to the correction to production vertex, as well as to interference between production and decay and even to interference between top decay and antitop decay, depending on when the top quark propagators are closer to the resonances. Moreover, the amplitudes in Eq. (4) are not gauge invariant one by one, although their sum is.

For purposes related to gauge invariance, and in order to be able to perform comparisons with the on-shell computation, it is desirable to decompose the total amplitude into gauge

invariant corrections to particular subprocesses, and interference between these. The aim is to rewrite Eq. (4) as:

$$\mathcal{M}^{vg} = \mathcal{M}_{prod} + \mathcal{M}_{tdec} + \mathcal{M}_{\bar{t}dec} + \mathcal{M}_{prod-tdec}^{intf} + \mathcal{M}_{prod-\bar{t}dec}^{intf} + \mathcal{M}_{tdec-\bar{t}dec}^{intf} \quad (22)$$

with each term being gauge invariant by itself.

To this end, it is necessary to decompose the amplitudes $\mathcal{M}_{tt}, \mathcal{M}_{tb} \dots$ into parts which contribute solely to corrections to production, decay, or interference. This decomposition will be based on the top and antitop propagator structure of the matrix element. Following the prescription used in [13], products of propagators which go on-shell in different regions of the phase space can be decomposed as follows:

$$\frac{1}{D(p_t)} \frac{1}{D(p_t - k)} = \frac{1}{D_0(p_t - k)} \frac{1}{D(p_t)} - \frac{1}{D_0(p_t - k)} \frac{1}{D(p_t - k)} \quad (23)$$

with

$$D(p) = p^2 - \bar{m}^2, \quad D_0(p - k) = (p - k)^2 - p^2 \quad (24)$$

In Eq. (23) the first term on the right hand side is considered as a contribution to the production process and the second one a contribution to the decay process. Furthermore, it is convenient to write the result in term of products of gauge invariant currents (in a manner similar to [16]). For example, the $\mathcal{M}_{b\bar{t}}$ amplitude can be written (using the extended soft gluon approximation):

$$\mathcal{M}_{b\bar{t}}(ESGA) = \frac{\alpha_s}{4\pi} \mathcal{M}_0 \int \frac{d^4 k}{i\pi^2} G_{\mu\nu}(k) \frac{-2p_{\bar{t}}^\mu}{D(p_{\bar{t}} + k)} \frac{2p_b^\nu}{D_0(p_b - k)} \frac{D(p_t)}{D(p_t - k)} \quad (25)$$

where $G_{\mu\nu}(k)$ is the gluon propagator in an arbitrary gauge. By using the currents:

$$j_{tdec}^{b, \mu} = \frac{2p_b^\mu}{D_0(p_b - k)} \frac{D(p_t)}{D(p_t - k)} \quad (26)$$

$$j_{prod}^{\bar{t}, \mu} = \frac{-2p_{\bar{t}}^\mu}{D_0(p_{\bar{t}} + k)} \quad , \quad j_{tdec}^{\bar{t}, \mu} = \frac{-2p_{\bar{t}}^\mu}{D_0(p_{\bar{t}} + k)} \frac{D(p_{\bar{t}})}{D(p_{\bar{t}} + k)}$$

the expression (25) can be written as:

$$\mathcal{M}_{b\bar{t}}(ESGA) = \frac{\alpha_s}{4\pi} \mathcal{M}_0 \int \frac{d^4 k}{i\pi^2} G_{\mu\nu}(k) (j_{prod}^{\bar{t}, \mu} - j_{tdec}^{\bar{t}, \mu}) j_{tdec}^{b, \nu} \quad (27)$$

where the first term in parentheses contributes to production-decay interference, and the second one contributes to decay-decay interference.

We can similarly define the currents:

$$j_{tdec}^{b, \mu} = \frac{-2p_b^\mu}{D_0(p_b + k)} \frac{D(p_{\bar{t}})}{D(p_{\bar{t}} + k)} \quad (28)$$

$$j_{prod}^{t, \mu} = \frac{2p_t^\mu}{D_0(p_t - k)} \quad , \quad j_{tdec}^{t, \mu} = \frac{2p_t^\mu}{D_0(p_t - k)} \frac{D(p_t)}{D(p_t - k)}$$

and the amplitudes for the other two interference diagrams can be written like:

$$\mathcal{M}_{t\bar{b}}(ESGA) = \frac{\alpha_s}{4\pi} \mathcal{M}_0 \int \frac{d^4k}{i\pi^2} G_{\mu\nu}(k) (j_{prod}^{t, \mu} - j_{tdec}^{t, \mu}) j_{tdec}^{\bar{b}, \nu} \quad (29)$$

$$\mathcal{M}_{b\bar{b}}(ESGA) = \frac{\alpha_s}{4\pi} \mathcal{M}_0 \int \frac{d^4k}{i\pi^2} G_{\mu\nu}(k) j_{tdec}^{b, \mu} j_{tdec}^{\bar{b}, \nu} \quad (30)$$

Contributions to interference between subprocesses do not come solely from the manifestly non-factorizable diagrams. The diagrams in which the gluon contributes to vertex or self-energy corrections (Fig. 3a)) also contain interference terms. Since the decomposition into purely vertex (or self-energy) corrections and interference corrections is not unique, we shall present our approach in some detail.

The amplitude for the vertex correction diagram with off-shell particles can be written as:

$$(\delta\Gamma)_{12} = \frac{\alpha_s}{4\pi} \int \frac{d^4k}{i\pi^2} G_{\mu\nu}(k) \gamma^\nu \frac{A(p_1, p_2) + k^\alpha B_\alpha(p_1, p_2) + k^\alpha k^\beta C_{\alpha\beta}(p_1, p_2)}{((p_1 - k)^2 - m_1^2) (p_2 + k)^2 - m_2^2)} \gamma_\nu \quad (31)$$

A corresponding on-shell approximation for this amplitude would be

$$(\delta\Gamma)_{os} = \frac{\alpha_s}{4\pi} \int \frac{d^4k}{i\pi^2} G_{\mu\nu}(k) \gamma^\nu \frac{A(p'_1, p'_2) + k^\alpha B_\alpha(p'_1, p'_2) + k^\alpha k^\beta C_{\alpha\beta}(p'_1, p'_2)}{(-2p'_1 k + k^2) (2p'_2 k + k^2)} \gamma_\nu \quad (32)$$

where p'_1 and p'_2 are some on-shell approximations for p_1 and p_2 ($p_1^2 = p_2^2 = m^2$). Now, we can define the interference contribution through:

$$(\delta\Gamma)_{12} = (\delta\Gamma)_{12}^{os} + (\delta\Gamma)_{12}^{intf} \quad (33)$$

Note, however, that $(\delta\Gamma)_{12}^{os}$ is not unique, since p'_1, p'_2 are not unique; different choices for these momenta would yield different results for $(\delta\Gamma)_{12}^{os}$. The uncertainty which arises is, of course, of order $p^2 - m^2$, so it can be neglected in the DPA. However, it allows us to choose the following definition for $(\delta\Gamma)_{12}^{os}$:

$$\begin{aligned} (\delta\Gamma)_{12}^{os} = & \frac{\alpha_s}{4\pi} \int \frac{d^4k}{i\pi^2} G_{\mu\nu}(k) \left[\frac{(2p_1^\mu) \Gamma(-2p_2^\nu)}{D_0(p_1 - k) D_0(p_2 + k)} \right. \\ & \left. + \gamma^\mu \frac{k^\alpha B_\alpha(p_1, p_2) + k^\alpha k^\beta C_{\alpha\beta}(p_1, p_2)}{D(p_1 - k) D(p_2 + k)} \gamma^\nu \right]. \end{aligned} \quad (34)$$

This choice means that the purely vertex correction (factorizable) part of the vertex diagram can be obtained by simply replacing the off-shell $C_0(p_1, p_2, 0, m_1, m_2)$ function appearing in the expression for $(\delta\Gamma)_{12}$ with the on-shell, infrared divergent function $C_0(p_1, p_2, \mu, \sqrt{p_1^2}, \sqrt{p_2^2})$.

Conversely, the interference part of the off-shell vertex correction diagram is:

$$(\delta\Gamma)_{12}^{intf} = \frac{\alpha_s}{4\pi} \int \frac{d^4k}{i\pi^2} G_{\mu\nu}(k) \left[\gamma^\mu \frac{A(p_1, p_2)}{D(p_1 - k) D(p_2 + k)} \gamma^\nu - \frac{(2p_1^\mu) \Gamma(-2p_2^\nu)}{D_0(p_1 - k) D_0(p_2 + k)} \right] \quad (35)$$

with $A(p_1, p_2) = (\not{p}_1 + m_1)\Gamma(-\not{p}_2 + m_2)$. For the $t\bar{t}$ production diagram, in DPA

$$\gamma^\mu(\not{p}_t + \bar{m}_t) \Gamma_{t\bar{t}}(-\not{p}_{\bar{t}} + \bar{m}_{\bar{t}})\gamma^\nu \rightarrow (2p_t^\mu) \Gamma_{t\bar{t}}(-2p_{\bar{t}}^\nu)$$

leading to

$$\mathcal{M}_{t\bar{t}}^{intf} = \frac{\alpha_s}{4\pi} \mathcal{M}_0 \int \frac{d^4k}{i\pi^2} G_{\mu\nu}(k) \left[(-j_{tdec}^{t, \mu}) j_{prod}^{\bar{t}, \nu} + j_{prod}^{t, \mu} (-j_{\bar{t}dec}^{\bar{t}, \nu}) + (-j_{tdec}^{t, \mu}) (-j_{\bar{t}dec}^{\bar{t}, \mu}) \right]. \quad (36)$$

Things are different for the decay vertex corrections, since we have doubly resonant contributions which are not proportional to the tree level matrix element. In the top decay case, the transformation:

$$\gamma^\mu(\not{p}_b + \bar{m}_b) \not{\epsilon}_{W^+}(\not{p}_t + \bar{m}_t)\gamma^\nu \rightarrow (2p_b^\mu) \not{\epsilon}_{W^+} [2p_t^\nu + \gamma^\nu(-\not{p}_t + \bar{m}_t)]$$

will lead to:

$$\mathcal{M}_{tb}^{intf} = \frac{\alpha_s}{4\pi} \int \frac{d^4k}{i\pi^2} G_{\mu\nu}(k) j_{tdec}^{b, \mu} \left[(-j_{prod}^{t, \nu}) \mathcal{M}_0 + M_1^{t, \nu} \right] \quad (37)$$

where

$$M_1^{t, \mu} = \frac{-1}{D(p_t) D(p_{\bar{t}})} \left[\bar{u}(b) \not{\epsilon}_{W^+} \gamma^\mu \Gamma_{\gamma, Z_0}(-\not{p}_{\bar{t}} + \bar{m}_{\bar{t}}) \not{\epsilon}_{W^-} v(\bar{b}) \right] \quad (38)$$

In a similar manner, the interference term $\mathcal{M}_{\bar{t}b}^{intf}$ coming from the antitop vertex correction diagram can be written in terms of the currents $j_{\bar{t}dec}^{\bar{b}, \mu}$, $-j_{prod}^{\bar{t}, \nu}$, and the matrix element $M_1^{\bar{t}, \nu}$.

Finally, the last diagrams to be split into on-shell and interference contribution are the top, antitop self-energy diagrams. Using the same approach as in the vertex case, we define:

$$\begin{aligned} (\Delta Z)_t^{intf} &= \frac{\alpha_s}{4\pi} \left\{ \int \frac{d^4k}{i\pi^2} G_{\mu\nu}(k) \left[\gamma^\mu \frac{\not{p}_t + \bar{m}_t}{D(p_t - k)} \gamma^\nu - \frac{2p_t^\mu \gamma^\nu}{D_0(p_t - k)} \right] \right\} \frac{\not{p}_t + \bar{m}_t}{D(p_t)} \\ &- (-1) \frac{\alpha_s}{4\pi} \int \frac{d^4k}{i\pi^2} G_{\mu\nu}(k) \frac{2p_t^\mu}{D_0(p_t - k)} \frac{2p_{\bar{t}}^\nu}{D_0(p_{\bar{t}} - k)} \end{aligned} \quad (39)$$

where the quantity in the curly brackets is the renormalized top self-energy, and the quantity on the second line is the on-shell limit of the quantity on the first line. This will lead to the following result for the interference contribution coming from the top self-energy diagram:

$$\mathcal{M}_{tt}^{intf} = \frac{\alpha_s}{4\pi} \int \frac{d^4k}{i\pi^2} G_{\mu\nu}(k) \left[j_{prod}^{t, \mu} \mathcal{M}_0 - M_1^{t, \mu} \right] j_{tdec}^{t, \nu} \quad (40)$$

and a similar one from the antitop self-energy diagram.

Now we have all the pieces needed to write down the interference terms. The final result is:

$$\begin{aligned} \mathcal{M}^{intf} &= \frac{\alpha_s}{4\pi} \int \frac{d^4k}{i\pi^2} G_{\mu\nu}(k) \left[(j_{prod}^\mu \mathcal{M}_0 + M_1^{t, \mu}) j_{tdec}^\nu - (j_{prod}^\mu \mathcal{M}_0 - M_1^{\bar{t}, \mu}) j_{\bar{t}dec}^\nu \right. \\ &\quad \left. + j_{tdec}^\mu j_{\bar{t}dec}^\nu \mathcal{M}_0 \right] \end{aligned} \quad (41)$$

It is easy in this formula to identify the production-decay or decay-decay interference terms. The currents:

$$j_{prod} = j_{prod}^{\bar{t}} - j_{prod}^t \quad , \quad j_{tdec} = j_{tdec}^b - j_{tdec}^t \quad , \quad j_{\bar{t}dec} = j_{\bar{t}dec}^{\bar{b}} - j_{\bar{t}dec}^{\bar{t}} \quad (42)$$

are conserved, and gauge invariant in DPA. Therefore, the total interference contribution as well as the interference between subprocesses parts are gauge invariant in the approximation used.

3 Computational Approach

Once a consistent scheme for evaluating the virtual corrections to the top production and decay process (1) has been set up (as described in the previous sections), the next step is the implementation of this scheme in a Monte Carlo program. In this section we give some details about the technical issues arising in the design of such a program, and how we choose to solve them.

There are two types of quantities involved in the evaluation of the NLO amplitude: scalar quantities (form factors), which encode the contribution of loops, and spinorial quantities, built from Dirac spinors and operators. For example, the contribution coming from the $t\bar{t}$ vertex correction can be written:

$$\tilde{\mathcal{M}}_{t\bar{t}} = \bar{u}(p_b) \not{\epsilon}_{W^+}(\not{p}_t + m_t) \delta\Gamma_{ren}^{t\bar{t}}(-\not{p}_{\bar{t}} + m_t) \not{\epsilon}_{W^-}v(p_{\bar{b}}) \quad (43)$$

or, using the decomposition in Eq. (12) :

$$\tilde{\mathcal{M}}_{t\bar{t}} = \frac{\alpha_s}{4\pi} \sum_{i=1,2} \left[C_V F_i^V T_i^V + C_A F_i^A T_i^A \right] \quad (44)$$

(for more details see [22]).

Let's start by discussing the evaluation of the scalar form factors F_i . Rather than compute analytic expressions for each form factor, we have chosen to evaluate them in terms of Passarino-Veltman (PV) functions [23]. This approach has the advantage that we have to compute only a few quantities which contain logarithms and dilogarithms: the \mathcal{B}_0 two-point and \mathcal{C}_0 three-point scalar functions (all the rest can be written as linear combinations of these functions). In turn, for evaluating the PV 2 and 3-point scalar functions, we use the FF routines [24].

To compute the amplitudes corresponding to the interference diagrams, we need to be able to evaluate the 4-point and 5-point scalar integrals in Eqs. (7), (9), (10). There are no published results (or routines) for the general (complex masses) 4-point scalar integrals. We have build such routines for the infrared finite \mathcal{D}_0 function by using the general methods described in [25]. The results of these routines have been checked against analytical results in the soft gluon approximation published in [18].

The 5-point scalar function \mathcal{E}_0 has been computed by reduction to 4-point functions, following the recipe in [16]. The resulting infrared divergent 4-point functions have been evaluated using the analytic results published in [26].

Some comments on the treatment of the top width are needed here. One way of evaluating the scalar form factors in Eq. (44) is to compute the gluon integrals in the zero top width limit and introduce the finite width only in terms which are divergent on-shell (that is, replace m_t^2 with $\bar{m}_t^2 = m_t^2 - im_t\Gamma_t$ in terms like $\log(p_t^2 - m_t^2)$; see for example [16]). The difference between this result and the one obtained by using the complex top mass in all the terms is of order Γ_t/m_t , therefore at about 1% level. This would be acceptable if the radiative corrections would be small with respect with the tree level result (as is the case for the W production process), but in our case it turns out that the one-loop QCD corrections are of the same order of magnitude as the tree level result⁸. Therefore, order % terms are important. Since in the case of real gluon radiation the top width appears in all terms, for reasons of consistency we need to keep the width in all terms in the evaluation of the virtual corrections too.

The other elements needed in the evaluation of the amplitude (44) are the spinor sandwiches T_i . We compute these quantities using spinor techniques, as for the real gluon radiation case. Since this part of the computation is quite complex, and hence prone to errors, we have two different ways of performing it. In one approach, we express the T_i 's in terms of basic spinor products $\bar{u}(p_i, s_i)u(p_j, s_j)$; this is the more involved case (in terms of the work done by the programmer), geared for implementation in a Fortran routine, and which allows fast computation. The other approach uses C++ routines which allow the automated evaluation of general spinor sandwiches like

$$\bar{u}(p, s)(\not{p}_1 + m_1)(\not{p}_2 + m_2) \dots u(p', s')$$

(To this purpose, we have constructed classes that describe $\langle bra|$ and $|ket \rangle$ spinors, and operators of type $\not{p}_i \pm m_i$; in turn, these classes use the basic classes - 4-vector, complex number - defined in the Pandora event generator [27]). This method allows easy evaluation of T_i expressions (again from the programmer's viewpoint) and is much more resistant to programming errors; but the computation is slower than in the previous method. Therefore, the main use of the results obtained from the C++ routines is to check the Fortran results.

4 On-shell DPA

The issue of interference effects in the production and decay of heavy unstable particles has been the subject of extensive studies in the past decade. One of the main results is the theorem, due to Fadin, Khoze and Martin [28], which states that these interference effects are suppressed (see also a more recent discussion in [29]). A stronger version of this theorem [30] claims that NLO interference effects cancel in inclusive quantities up to terms of order $\alpha\Gamma/M$. As in [30], it is possible to define and use a framework for the computation of interference corrections in which the total interference contribution to inclusive quantities is zero.

In order to facilitate a comparison with our results (where the interference contributions do not cancel completely), we shall discuss this alternative approach (which we shall call on-

⁸The reason the *total* QCD corrections are of order 10 - 20% is because of large cancellations between the virtual corrections and soft gluon real corrections.

shell DPA) in some detail. Results obtained using on-shell DPA have been obtained for the W pair production case at LEP II ([16], [18]), as well as, more recently, for the evaluation of interference (non-factorizable) corrections to the top production and decay process at e^+e^- and hadron colliders [12].

The relevant features of this approach are two: first, the amplitudes for corrections to subprocesses are computed in the on-shell approximation for the top quarks. For example, the correction to the production process can be written in terms of the on-shell amplitude:

$$\tilde{\mathcal{M}}_{prod}^{os} = \sum_{\lambda, \lambda'} \mathcal{M}_{\lambda, \lambda'}(e^+e^- \rightarrow t\bar{t}(g)) \mathcal{M}_{\lambda}(t \rightarrow bW^+) \mathcal{M}_{\lambda'}(\bar{t} \rightarrow \bar{b}W^-) \quad (45)$$

where λ, λ' are the spins of the top quarks. The difference between the above amplitudes and the ones used in this paper (Eqs. (22), (34)) is due to non-doubly resonant terms, therefore acceptable in DPA.

The other characteristic feature of the on-shell DPA method is that the interference due to real gluon radiation is computed by using a semianalytic approach. This approach rests on the observation that interference is due mainly to gluons of energies of order Γ_t ; therefore, the (extended) soft gluon approximation can be employed for the evaluation of interference terms.

There are two stages where this approximation comes into play. First, it is used at the matrix element evaluation level. For example, consider interference between the diagrams where the gluon is radiated from the bottom quark and from the antitop quark:

$$\begin{aligned} d\sigma_{tb}^{rg}(p_b, p_W, \dots, k) &\sim 2\text{Re} \left[\sum_{\epsilon_g} \mathcal{M}_b^{sg} (\mathcal{M}_{\bar{t}}^{sg})^* \right] \\ &= |\mathcal{M}_0(p_b, p_W, \dots)|^2 2\text{Re} \left[\frac{4p_{\bar{t}}p_b}{2kp_b + i\epsilon} \frac{p_t^2 - \bar{m}_t^2}{(p_t + k)^2 - \bar{m}_t^2} \frac{1}{(p_{\bar{t}} + k)^2 - \bar{m}_t^{2*}} \right]. \end{aligned} \quad (46)$$

The second stage is the treatment of the final state phase space. In the soft gluon approximation, it factorizes: $d\Omega_{b,W,\dots,g} = d\Omega_{b,W,\dots} \times d\Omega_g$, and the integration over the gluon momenta is performed separately:

$$\begin{aligned} d\sigma_{tb}^{rg}(p'_b, p'_W, \dots) &= |\mathcal{M}_0(p'_b, p'_W, \dots)|^2 \\ &\times \frac{\alpha_s}{\pi} \text{Re} \left[\int \frac{d^3k}{2\pi\omega} \frac{4p_{\bar{t}}p_b}{2kp_b + i\epsilon} \frac{p_t^2 - \bar{m}_t^2}{(p_t + k)^2 - \bar{m}_t^2} \frac{1}{(p_{\bar{t}} + k)^2 - \bar{m}_t^{2*}} \right] \end{aligned} \quad (47)$$

where p'_b, p'_W, \dots are given by a suitable projection of the off-shell momenta p_b, p_W, \dots onto the on-shell phase space (for an example of how this projection might be accomplished see [31]). In the above equation $p_t = p'_b + p'_{W+}$, $p_{\bar{t}} = p'_b + p'_{W-}$, and the integral over gluon momenta is allowed to go to infinity (since hard gluons contribute nonresonant terms to the result).

The quantity on the second line of Eq. (47) can be evaluated analytically, through methods similar to those used to evaluate the virtual 4-point functions. We will not give the results here (they can be found in [16], [18]), but there is an important comment to make.

Using this procedure to compute the real gluon interference, the total interference obtained by adding the virtual diagram contribution (Eq. (7)) to the above result and integrating over the top invariant mass parameter is zero [30]. This cancellation works also for the other interference diagrams; therefore, in this approach, the contribution of non-factorizable corrections is zero to the total cross section. However, this result depends on two things. First, it requires an inclusive treatment of real gluon radiation, with phase space integration extending to infinity. Second, both the virtual and the real interference terms have to be treated in the soft gluon approximation.

But, is the use of the soft gluon approximation justified in this case? At the amplitude level (Eq. (46)), the answer is yes; the relevant gluon energy, being of order Γ_t , is much smaller than the other momenta involved. However, this approximation does not seem to be acceptable for the phase space factorization stage of the above approach. Here, problems might arise when projecting the off-shell momenta onto the on-shell phase space. The reason is that there is no single way to perform this projection; therefore, in the determination of the on-shell momenta p'_b, p'_W, \dots there is an uncertainty of the order of the gluon energy, or Γ_t . Now, being close to the top resonances, we are in a region of the phase space where the cross section varies greatly over a range of energy of order Γ_t (due to the top quark propagators); therefore such an uncertainty is not acceptable.

To illustrate the dependence of the result for real gluon interference on the choice of the on-shell momenta p'_b, p'_W, \dots , let's presume that instead of projecting p_b into p'_b , we also take into account the gluon momentum: $p_b + k \rightarrow p'_b$ (physically, this might be justified by the inclusion of the gluon jet in the bottom quark jet). Then, Eq. (47) becomes:

$$d\sigma_{tb}^{rg}(p'_b, p'_W, \dots) = |\mathcal{M}_0(p'_b, p'_W, \dots)|^2 \frac{\alpha_s}{\pi} \text{Re} \left[\int \frac{d^3k}{2\pi\omega} \frac{4p_{\bar{t}}p_b}{2kp_b + i\epsilon} \frac{1}{(p_{\bar{t}} + k)^2 - \bar{m}_t^{2*}} \right] \quad (48)$$

The result for the above expression is different from the result for Eq. (47), and the difference contains doubly resonant terms. Therefore, in the on-shell DPA approach, the result for the interference terms depends on the choice of the implementation of the phase space factorization. A discussion of this dependence for the W pair production case can be found in [16].

5 Results for virtual corrections and the total cross section

In this section, we present some results on the total cross section for the top production and decay process at linear colliders. We take into account the virtual corrections as well as contributions coming from real gluon radiation. Furthermore, we study the effect of interference (nonfactorizable) terms on invariant top mass distributions and we perform comparisons with results previously published [12].

In obtaining the results presented in this section, the following set of parameters is used:

$$m_t = 175 \text{ GeV}, \quad \alpha_s = 0.1, \quad \Gamma_t^0 = 1.55 \text{ GeV}, \quad \Gamma_t = 1.42 \text{ GeV},$$

where Γ_t^0 is the top width at the tree level, while Γ_t includes the NLO QCD radiative corrections.

We start by looking at the total cross section for our process. Table 1 presents results for the following quantities:

- σ_0 : cross section for the tree level process (2); computed in the on-shell (narrow width) approximation, using the zero-order top width Γ_t^0 .
- σ_1^{os} : cross section for the NLO process in the on-shell approximation; computed using the NLO top width Γ_t .
- σ_1^{fact} : the main (factorizable) part of the DPA approximation to the NLO process. This quantity contains corrections to production and decay as defined in section 2.4.
- σ_1^{intf} : the interference (non-factorizable) part of the DPA approximation to the NLO process, as defined in section 2.4.

	360 GeV	500 GeV	1000 GeV
$\sigma_0(pb)$	0.386	0.570	0.172
$\sigma_1^{os}(pb)$	0.700(1)	0.660(2)	0.1839(7)
$\sigma_1^{fact}(pb)$	0.676(2)	0.664(2)	0.1920(8)
$\sigma_1^{intf}(pb)$	-0.032(1)	-0.0116(3)	-0.0061(2)

Table 1: Total cross sections for top production at linear colliders with no cuts on phase space (numbers in parantheses are errors due to numerical integration).

We present results for three values of collision center-of-mass energies: 360 GeV, just above the $t\bar{t}$ production threshold, 500 GeV, the most common value used in linear collider studies, and 1 TeV, which is relevant for higher energy machines. The 360 GeV result is probably not good; this close to the threshold, resummation of large logarithms appearing in the $t\bar{t}$ interaction is needed [2]. However, it is interesting to see the magnitude of the nonfactorizable corrections at fixed order in this energy range.

The NLO cross sections contain contributions from the virtual corrections as well as from real gluon radiation (evaluated as in [13]). The phase space splicing method is used for the treatment of infrared singularities. The value of the technical cut which separates the infrared from the real gluons is $\epsilon = 0.1$ GeV; the results are independent of the choice of this parameter⁹. No physical cuts have been imposed on the final phase space.

The results in Table 1 prompt several comments. First, the difference between σ_1^{os} and σ_1^{fact} is due to non-doubly-resonant terms, therefore it could be expected to be small. This is indeed the case at 500 GeV; but at 1 TeV, this difference is about 4% of the cross section. The reason is that in obtaining these results, we have integrated over the complete kinematic

⁹Taking its value much smaller than the top width allows the use of the soft gluon approximation and phase space factorization in the evaluation of the infrared integrals.

range available for the top quark invariant mass (that is, $m_b + m_W < \sqrt{p_t^2} < W - (m_b + m_W)$), so the cross-sections include contributions from regions of the phase space where the top quarks are far off-shell and non-resonant terms are important.

	360 GeV	500 GeV	1000 GeV
$\sigma_1^{os}(pb)$	0.682(1)	0.627(2)	0.1742(7)
$\sigma_1^{fact}(pb)$	0.670(2)	0.629(2)	0.1781(5)
$\sigma_1^{intf}(pb)$	-0.034(1)	-0.0068(2)	-0.0017(1)

Table 2: Total cross sections for top production at linear colliders with cuts on the top, antitop invariant mass.

In Table 2 we present the cross section results obtained with a cut on the t, \bar{t} invariant mass $|\sqrt{p_t^2}, \sqrt{p_{\bar{t}}^2} - m_t| < 15$ GeV. The difference between the two results for the main terms σ_1^{os} and σ_1^{fact} is smaller in this case. Note that, since in the on-shell approach $p_t^2, p_{\bar{t}}^2 = m_t^2$, σ_1^{os} in Table 1 and 2 contains a factor which simulates the effect of cuts (either from kinematic constraints or imposed ones) on the top invariant mass. Note also that these cuts are not imposed *ad hoc*, but they arise rather naturally in the process of defining a t, \bar{t} production event; it makes sense to require that the reconstructed mass of the b, W pairs is close to the top mass in the definition of such an event. In this context, it is also worth noting that the contribution coming from the phase space region where either the t or \bar{t} is far off-shell (more than ten times the width) is quite sizable (around 5% of the total cross section for center-of-mass energies greater than 500 GeV).

Another quantity of interest is the differential interference cross section as a function of the top invariant mass. Even if the total interference contribution to the cross section is small (at about 1% level), it can have larger effects in differential distributions since it can be positive in certain regions of the phase space and negative in others. In particular, it can be important in the reconstruction of the top invariant mass; since $d\sigma_1^{intf}$ tends to decrease as $\sqrt{p_t^2}$ increases, the net effect would be to shift the position of the Breit-Wigner peak to smaller invariant mass values. This effect can be quantified by the following equation: the shift in the mass is

$$\Delta M_t = \left(\frac{d\delta_{nf}}{dM_t} \right) \bigg|_{M_t=m_t} \frac{\Gamma_t^2}{8} \quad (49)$$

where $M_t = \sqrt{p_t^2}$, and δ_{nf} is the ratio of the non-factorizable (interference) part of the cross section to the Born cross section:

$$\delta_{nf} = \frac{d\sigma_1^{intf}}{d\sigma_0}$$

In Figure 6 we present the differential distribution for the relative non-factorizable correction $\delta_{nf}(M_t)$ at center of mass energy 500 GeV. The dashed line is the result which takes into account the full interference corrections in Eq. (41); the solid line is obtained by taking into account only the terms proportional to the Born amplitude. Note that, although the contribution of the M_1 terms in Eq. (41) to the total cross section is very close to zero,

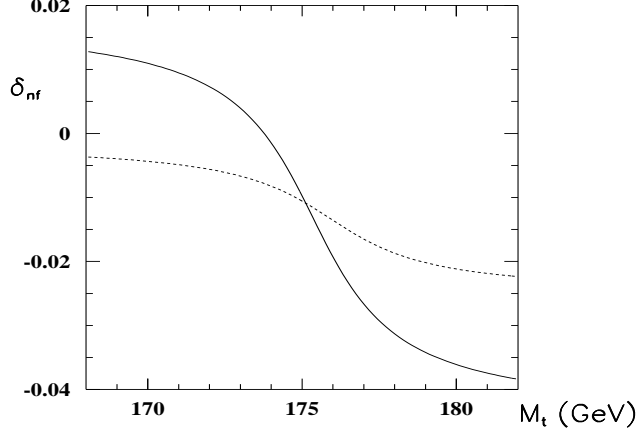


Figure 6: The relative nonfactorizable correction to the invariant mass distribution; the solid line is the contribution of terms proportional to the tree level amplitude, while the dashed line contains also the M_1 terms in Eq. (41).

they have a sizable effect on the differential distribution in Fig. 6. Using Eq. (49), we conclude that the shift in the position of the peak in the top invariant mass distribution due to interference effects is very small (of order of a few MeV – in agreement with [12]).

The results in Table 1 and 2 indicate that the contribution of interference terms to the total cross section is of order 1%, in agreement with the Γ_t/m_t order of magnitude expected from naive arguments. However, it is not zero, as implied by results presented in [12], which use the on-shell DPA method. We have argued in section 4 that this difference is due to the way in which the radiation of real gluon with energies of order Γ_t is treated. In Figure 7, we

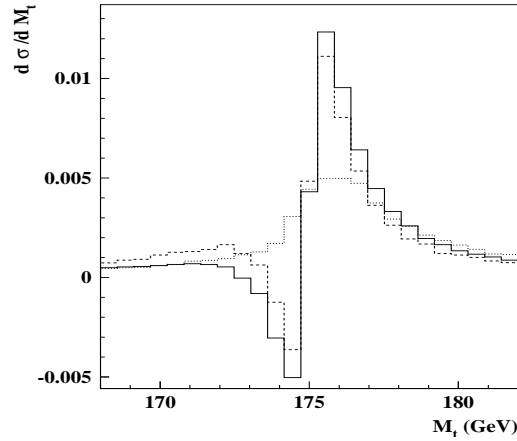


Figure 7: Real gluon interference: the $\sigma_{b\bar{t}}$ term. The solid line corresponds to the semianalytic approach; the dashed line is obtained through numerical evaluation with $M_t = \sqrt{p_{bW}^2}$; the dotted line is obtained through numerical evaluation with M_t given by Eq. (50).

present the results for the real interference between the diagram where the gluon is radiated from the bottom quark and the diagram where the gluon is radiated from the antitop quark. The solid line is the result of the semianalytical approach described in section 4. The other two lines are the result of the exact off-shell computation (where the integration over the gluon momenta is performed numerically). The two lines correspond to two different ways in which the gluon momentum is treated in the reconstruction of the invariant top mass. For the dashed line, the gluon momentum is ignored in the top mass reconstruction: $M_t = \sqrt{p_{bW}^2}$. Note that in this case, the result is quite close to that of the semianalytical computation, which is natural, since the gluon momentum is treated in both cases the same way.

To obtain the dotted line, we have followed a more realistic approach, in which the gluon is included in the top mass reconstruction if it happens to be radiated close enough to the top quark:

$$M_t = \begin{cases} \sqrt{p_{bWg}^2} & \text{if } \cos\theta_{tg} < \pi/3 \\ \sqrt{p_{bW}^2} & \text{otherwise} \end{cases} \quad (50)$$

Although the total cross section is the same as for the other exact evaluation case, the differential cross section differs by quite a bit.

The total cross section corresponding to the interference term presented in Figure 7 has the value $\sigma_{b\bar{t}} = 0.121 \text{ pb}$ for the semianalytical result, and $\sigma_{b\bar{t}} = 0.124 \text{ pb}$ for the numerical one. Note that, since the diagram set contributing to this interference term is not gauge invariant, this result has no physical meaning by itself. However, from these numbers we can get some insight concerning the evaluation of interference corrections. First, note that the contribution of this single diagram is much bigger (about two orders of magnitude) than the total result for the interference terms. This means that there are large cancellations taking place between the real and virtual interference contributions. This is quite natural, in accordance with the discussion in section 4; however, this also means that small uncertainty (order percent) in evaluating one of this contributions (the one coming from the real

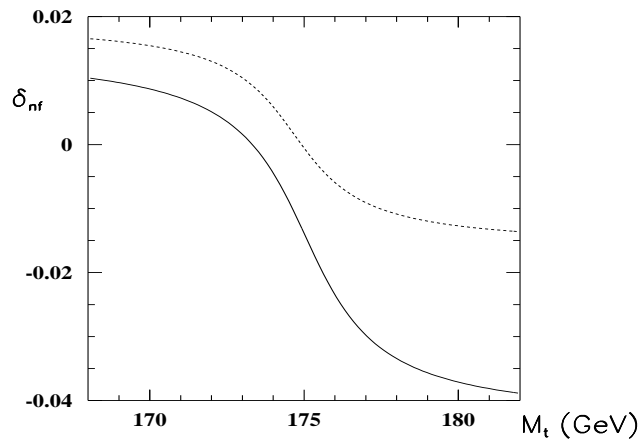


Figure 8: The relative nonfactorizable correction to the invariant mass distribution; comparison between the semianalytical (dashed line) and the numerical (solid line) approach.

gluon interference, for example) can lead to large uncertainties in the evaluation of the total interference contribution.

In Figure 8 we present the comparison between the relative non-factorizable corrections computed in the semianalytical approximation (dashed line) and the complete off-shell approach (solid line). For the purpose of this comparison, we consider only the terms proportional to the Born amplitude in the exact computation, since only these terms are taken into account in the semianalytical approach. Note that the total interference cross section integrates to zero in the latter case, and, as discussed above, the complete off-shell distribution contains contributions that do not cancel in the total cross section.

6 Conclusions

In this paper, we have discussed in some detail the evaluation of next to leading order QCD corrections to the top production and decay process at a linear collider. Since a full computation of the NLO amplitudes contributing to the process $e^+e^- \rightarrow b W^+ \bar{b} W^-$ is not feasible, the double pole approximation (DPA) has been employed. In our case this means taking into account only the diagrams which contain two intermediate top quarks. Unlike most of the previous treatments, we allow for the two top quarks to be off-shell, and include also the corrections due to interference between the top production and decay processes.

A parallel is drawn between our computation and the DPA evaluation of QED corrections to the W pair production and decay process at LEP. While there are many similarities between the two computations, there are also some differences; the most striking one is that there are nonfactorizable (interference) corrections no longer proportional to the Born amplitude in the top quark case. Although the contribution of these terms to the total cross section (or other inclusive quantities) is consistent with zero, they contribute to differential distributions.

Previous results obtained using a semianalytical approach state that the interference terms cancel out completely in inclusive quantities (like the total cross section). We discuss the evaluation of the real gluon interference terms using analytic methods and we point out the shortcomings of this approach. The total magnitude of nonfactorizable corrections in our computation is found to be of order 1% of the cross section. We also present results for the total cross section and the relative nonfactorizable correction to the top invariant mass distribution. The effect of nonfactorizable corrections on the top mass reconstruction is found to be very small.

The results presented in this paper are relevant at collision energies above the top - antitop production threshold. Since we are interested in differential distributions of final state kinematic variables, the approach used to obtain cross section distributions is that of numerical simulations. The amplitudes are evaluated using spinor techniques, and the integration over the final state variables is performed using Monte Carlo techniques. This approach has the added advantage that it allows for the inclusion of experimentally relevant selection criteria on the final state phase space.

The calculation presented here is entirely at the parton level. For more realistic simulations, it is necessary to take into account initial state related issues, like initial state

radiation (ISR), beam energy spread and beamstrahlung. The hadronization of the final state partons also has to be modeled. Further extensions of interest include taking into account singly-resonant diagrams (tree level as well as NLO in the on-shell approximation) and the evaluation of electroweak corrections.

Acknowledgments

I would like to thank Prof. L.H. Orr for support during the completion of this work and for suggesting the topic in the first place. Also, many thanks to D. Wackerroth for discussions about the evaluation of electroweak corrections to the W pair production and decay process, to A.P. Chapovsky for help with the numerical comparisons with previous results, and to O.I. Yakovlev for clarifying some issues related to the DPA.

This work was supported in part by the U.S. Department of Energy, under grants DE-FG02-91ER40685 and DE-FG03-98ER-41076, and by the U.S. National Science Foundation, under grant PHY-9600155.

Appendix

In this appendix we shall give some details about the evaluation of vertex corrections and fermion self energies. For a more extensive description, we refer the reader to [22].

The amplitude for the general vertex correction in Figure 4 can be written as:

$$\delta\Gamma^\mu = \frac{\alpha_s}{4\pi} \int \frac{d^4k}{i\pi^2} \frac{1}{k^2} \gamma^\nu \frac{\not{p}_1 - \not{k} + m_1}{(p_1 - k)^2 - \bar{m}_1^2} \gamma^\mu (C_V + C_A \gamma^5) \frac{-\not{p}_2 - \not{k} + m_2}{(p_2 + k)^2 - \bar{m}_2^2} \gamma_\nu \quad (51)$$

Upon evaluation of the integral, the result can be written in terms of two sets of form-factors; one for the vectorial part of the vertex correction, one for the axial part. The number of form factors needed depends on the specific constraints on the process; in the general case, when the momenta p_1, p_2 are off-shell, eight $\times 2$ form factors are involved:

$$\delta\Gamma^\mu = \frac{\alpha_s}{4\pi} \sum_{i=1,8} \left(C_V F_i^V T_i^{V\mu} + C_A F_i^A T_i^{A\mu} \right) \quad (52)$$

The definition of these form factors depends on the choice of the spinorial elements in terms of which the result is written. We define:

$$\delta\Gamma_V^\mu = \frac{\alpha_s}{4\pi} C_V \times \quad (53)$$

$$\begin{bmatrix} p_1^\mu & F_1^V & + & \gamma^\mu & F_2^V & + \\ (\not{p}_1 - m_1) & p_1^\mu & F_3^V & + & (\not{p}_1 - m_1) & \gamma^\mu & F_4^V & + \\ & p_1^\mu & (-\not{p}_2 - m_2) & F_5^V & + & \gamma^\mu & (-\not{p}_2 - m_2) & F_6^V & + \\ (\not{p}_1 - m_1) & p_1^\mu & (-\not{p}_2 - m_2) & F_7^V & + & (\not{p}_1 - m_1) & \gamma^\mu & (-\not{p}_2 - m_2) & F_8^V \end{bmatrix}$$

for the vectorial part of the vertex correction; for the axial one, replace p_1^μ , γ^μ with $p_1^\mu \gamma^5$, $\gamma^\mu \gamma^5$ in the expression above. This definition has the advantage that when the particle i is on-shell, the terms which contain the $\pm \not{p}_i + m_i$ drop out. Also, we have made use of the fact

that, if $\delta\Gamma^\mu$ multiplies A_μ in the full matrix element (A_μ can be thought of as the polarization vector of the gauge boson in diagram 4), then $(p_1 + p_2)^\mu A_\mu = 0$.

We shall evaluate and write the results for the form factors in terms of Passarino - Veltman functions (for the definition of these see below):

$$\begin{aligned}
F_1^V &= 4[m_1(C_{12} - C_{11} + C_{23} - C_{21}) - m_2(C_{12} + C_{23})] \\
F_2^V &= -2[2p_1p_2(C_0 + C_{11}) + 2(C_{24} - 1/4) + 2B_0^{12} - 1 \\
&\quad - m_1m_2C_{11} + p_1^2(-C_{11} + C_{12}) - p_2^2C_{12}] \\
F_3^V &= -4(C_0 + 2C_{11} - C_{12} + C_{21} - C_{23}) \quad , \quad F_4^V = 2m_2(C_0 + C_{11}) \\
F_5^V &= -4(C_0 + C_{11} + C_{23} + C_{12}) \quad , \quad F_6^V = 2m_1(C_0 + C_{11}) \\
F_7^V &= 0 \quad , \quad F_8^V = 2(C_0 + C_{11})
\end{aligned} \tag{54}$$

In the computation of the axial form factors, γ^5 can be shifted to the right in Eq. (51). In the result for the form factors, this amounts to changing the sign of m_2 , $m_2 \rightarrow -m_2$, and multiplying the F_5, \dots, F_8 with (-1) . Then :

$$\begin{aligned}
F_1^A &= F_1^V + 8m_2(C_{12} + C_{23}) \quad , \quad F_2^A = F_2^V - 4m_1m_2C_{11} \\
F_3^A &= F_3^V \quad , \quad F_4^A = -F_4^V \\
F_5^A &= -F_5^V \quad , \quad F_6^A = -F_6^V \\
F_7^A &= -F_7^V \quad , \quad F_8^A = -F_8^V
\end{aligned} \tag{55}$$

The result (21) for the fermion self-energy corrections can be similarly written in terms of Passarino-Veltman functions:

$$\begin{aligned}
\Sigma_a(p^2) &= \frac{\alpha_s}{4\pi}(1 + 2B_1(p^2, \bar{m}^2)) \\
\Sigma_{ir}(p^2) &= \frac{\alpha_s}{4\pi} \frac{m^2}{p^2 - \bar{m}^2} \left[4\Delta B_0(p^2, \bar{m}^2) + 4\Delta B_1(p^2, \bar{m}^2) \right]
\end{aligned} \tag{56}$$

with

$$\Delta B_n(p^2, \bar{m}^2) = B_n(p^2, \bar{m}^2) - B_n(\bar{m}^2, \bar{m}^2) \quad , \quad n = 0, 1$$

If we further define the X_0, X_1 form factors through:

$$\Delta Z_2(p) = 2 \frac{\alpha_s}{4\pi} \left[X_0(p^2) + X_1(p^2)(\pm \not{p} - m) \right] \tag{57}$$

the renormalized vertex correction in Eq. (16) can be obtained by making the following redefinitions of form-factors in Eqs. (54), (55):

$$\begin{aligned}
F_2^{V,A} &\rightarrow F_2^{V,A} + X_0(p_1^2) + X_0(p_2^2) \\
F_4^{V,A} &\rightarrow F_4^{V,A} + X_1(p_1^2) \\
F_6^{V,A} &\rightarrow F_6^{V,A} + X_1(p_2^2)
\end{aligned} \tag{58}$$

These general results are easily translated for the specific cases which appear in our computation. For corections to the production, top decay and antitop decay vertices we have, respectively:

$$\begin{aligned} F_{i,\bar{t}\bar{t}}^{V,A} &= F_i^{V,A}(p_1 = p_t, p_2 = p_{\bar{t}}, m_1 = m_2 = m_t) \\ F_{i,tb}^{V,A} &= F_i^{V,A}(p_1 = p_b, p_2 = -p_t, m_1 = m_b, m_2 = m_t) \\ F_{i,\bar{t}\bar{b}}^{V,A} &= F_i^{V,A}(p_1 = -p_{\bar{t}}, p_2 = p_{\bar{b}}, m_1 = m_t, m_2 = m_b) \end{aligned} \quad (59)$$

The statndard definition for the (3-point) Passarino-Veltman functions is:

$$\mathcal{C}^{\{0,\mu,\mu\nu\}} = \int \frac{d^4k}{i\pi^2} \frac{\{1, k^\mu, k^\mu k^\nu\}}{(k^2 - m_1^2) ((k + p_1)^2 - m_2^2) ((k + p_1 + p_2)^2 - m_3^2)} \quad (60)$$

with the scalar functions $\mathcal{C}_{ij}(p_1^2, p_2^2, m_1^2, m_2^2, m_3^2)$ given by:

$$\begin{aligned} \mathcal{C}^\mu &= p_1^\mu \mathcal{C}_{11} + p_2^\mu \mathcal{C}_{12} \\ \mathcal{C}^{\mu\nu} &= p_1^\mu p_1^\nu \mathcal{C}_{21} + p_2^\mu p_2^\nu \mathcal{C}_{22} + (p_1^\mu p_2^\nu + p_2^\mu p_1^\nu) \mathcal{C}_{23} + g^{\mu\nu} \mathcal{C}_{24} \end{aligned} \quad (61)$$

The expressions for the reduction of \mathcal{C}_{ij} functions in terms of the scalar one-, two- and three-point integrals $\mathcal{A}^0, \mathcal{B}^0, \mathcal{C}^0$ are standard, and we do not give them here (see [22] or [32]).

The C function used in Eqs. (54), (55) are defined by:

$$C^{\{0,\mu,\mu\nu\}} = \int \frac{d^4k}{i\pi^2} \frac{\{1, k^\mu, k^\mu k^\nu\}}{(k^2 + i\epsilon) ((k - p_1)^2 - m_1^2) ((k + p_2)^2 - m_2^2)} \quad (62)$$

$$\begin{aligned} C^\mu &= -p_1^\mu C_{11} + (p_2 - p_1)^\mu C_{12} \\ C^{\mu\nu} &= p_1^\mu p_1^\nu C_{21} + (p_2 - p_1)^\mu (p_2 - p_1)^\nu C_{22} - [p_1^\mu (p_2 - p_1)^\nu + (p_2 - p_1)^\mu p_1^\nu] C_{23} \\ &\quad + g^{\mu\nu} C_{24} \end{aligned} \quad (63)$$

therefore:

$$C_0, C_{ij} = \mathcal{C}^0, \mathcal{C}_{ij}(p_1^2, (p_2 - p_1)^2, 0, m_1^2, m_2^2). \quad (64)$$

Moreover, the function B_0^{12} in Eq. (54) is given by:

$$B_0^{12} = \mathcal{B}^0((p_1 + p_2)^2, m_1^2, m_2^2) \quad (65)$$

and in Eqs. (56):

$$B_n(p^2, m^2) = \mathcal{B}_n(p^2, 0, m^2), \text{ for } n = 0, 1. \quad (66)$$

References

- [1] T. Abe et al., [American Linear Collider Working Group Collaboration], *Resource book for Snowmass 2001, 30 Jun - 21 Jul 2001, Snowmass, Colorado* SLAC-570, hep-ex/0106057, hep-ex/0106058
- [2] A. H. Hoang et al., Eur. Phys. J. Direct **C3** (2000) 1
- [3] B. Grzadkowski and Z. Hioki, Nucl. Phys. **B585** (2000) 3, Phys. Rev. **D 61** (2000) 014013, and Phys. Lett. **B476** (2000) 87
- [4] J. Jersak, E. Laerman, and P. Zerwas, Phys. Rev. **D 25** (1982) 1218
- [5] J.G.Korner, A.Pilaftsis, and M.M. Tung, Z. Phys. C **63** (1994) 575
- [6] J. Kodaira, T. Nasuno, and S. Parke Phys. Rev. **D 59** (1999) 014023
- [7] A. Brandenburg, M. Flesch, and P. Uwer, Phys. Rev. **D 59** (1999) 014001
- [8] M. Jezabek and J.H. Kuhn, Nucl. Phys **B314** (1989) 1
- [9] A. Czarnecki, Phys. Lett. **B252** (1990) 467
- [10] C.S. Li, R.J. Oakes, and T.C. Yuan, Phys. Rev. **D 43** (1991) 3579
- [11] C. R. Schmidt, Phys. Rev. **D 54** (1996) 3250
- [12] W. Beenakker, F. A. Berends, and A. P. Chapovsky, Phys. Lett. **B454** (1999) 129
- [13] C. Macesanu and L. H. Orr, Phys. Rev. **D 65** (2002) 014004
- [14] C. Macesanu and L.H. Orr, in 'Montreal 1998: Toward the Theory of Everything ', MRST'98 conference proceedings, p. 28-36; C. Macesanu and L.H. Orr, talk given at the APS Meeting of the Division of Particles and Fields (DPF 99), Los Angeles, CA, 5-9 Jan 1999, hep-ph/9906326
- [15] A. Denner, S. Dittmaier, M. Roth and D. Wackeroth, Nucl. Phys. **B560** (1999) and Nucl. Phys. **B587** (2000) 67
- [16] A. Denner, S. Dittmaier, and M. Roth, Nucl. Phys. **B519** (1998) 39
- [17] K. Melnikov and O. I. Yakovlev, Nucl. Phys. **B471** (1996) 90
- [18] W. Beenakker, F. A. Berends, and A. P. Chapovsky, Phys. Lett. **B411** (1997) 203 and Nucl. Phys. **B508** (1997) 17
- [19] T. Stelzer and W. F. Long, Comp. Phys. Comm. **81** (1994) 357
- [20] K. Kolodziej, hep-ph/0110063
- [21] V.A. Khoze, L.H. Orr, and W.J. Stirling, Nucl. Phys. **B378** (1992) 413

- [22] C. Macesanu, University of Rochester, Ph. D. dissertation (2001), hep-ph/0112035
- [23] G. Passarino and M. Veltman, Nucl. Phys. **B160** (1979) 151
- [24] G.J. van Oldenborgh, Comp. Phys. Comm. **66** (1991) 1
- [25] G. 't Hooft and M. Veltman, Nucl. Phys. **B153** (1979) 365.
- [26] W. Beenakker and A. Denner, Nucl. Phys. **B338** (1990) 349
- [27] M.E. Peskin, SLAC-PUB-8290, hep-ph/9910519
- [28] V.S. Fadin, V.A. Khoze and A.D. Martin, Phys. Lett. **B320** (1994) 141
- [29] A.P. Chapovsky, V.A. Khoze, A. Signer and W.J. Stirling, hep-ph/0108190
- [30] V.S. Fadin, V.A. Khoze and A.D. Martin, Phys. Rev. **D 49** (1994) 2247
- [31] W. Beenakker, F. A. Berends, and A. P. Chapovsky, Nucl. Phys. **B548** (1999) 3
- [32] K. Hagiwara, C.S. Kim, D. Haidt and S. Matsumoto, Z. Phys. C **64** (1994) 559